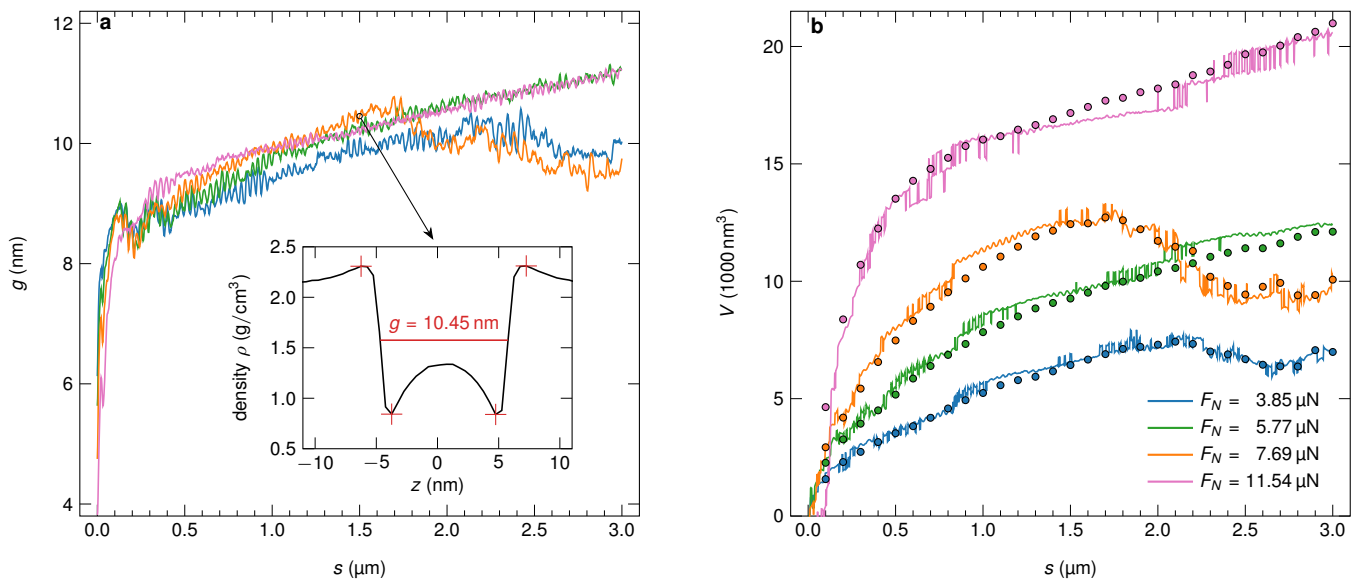# Effect of wear particles and roughness on nanoscale friction

Tobias Brink, Enrico Milanese, and Jean-François Molinari

Figure S1: Tribolayer thickness and wear volume calculated from density profiles. **a**, Thickness g of the tribolayer. The continued growth in the rolling regime is in accordance with the agglomeration of mass in the rolling wear particles. It can be seen that the tribolayer width stagnates together with the wear rate in the shear-band-like regime after around $s = 2\,\mu m$ for $F_N = 3.85\,\mu N$ and $7.69\,\mu N$. Inset: Calculation of g from a density profile in z direction (normal to the surfaces). **b**, Wear volume calculated by integrating over the density profile (lines) compared to the computation using the number of atoms in the tribolayer after separation (data points). The lines are shifted to zero at the beginning of the sliding simulation since the integrals include the initial wear particles, which we do not count in the wear volume.
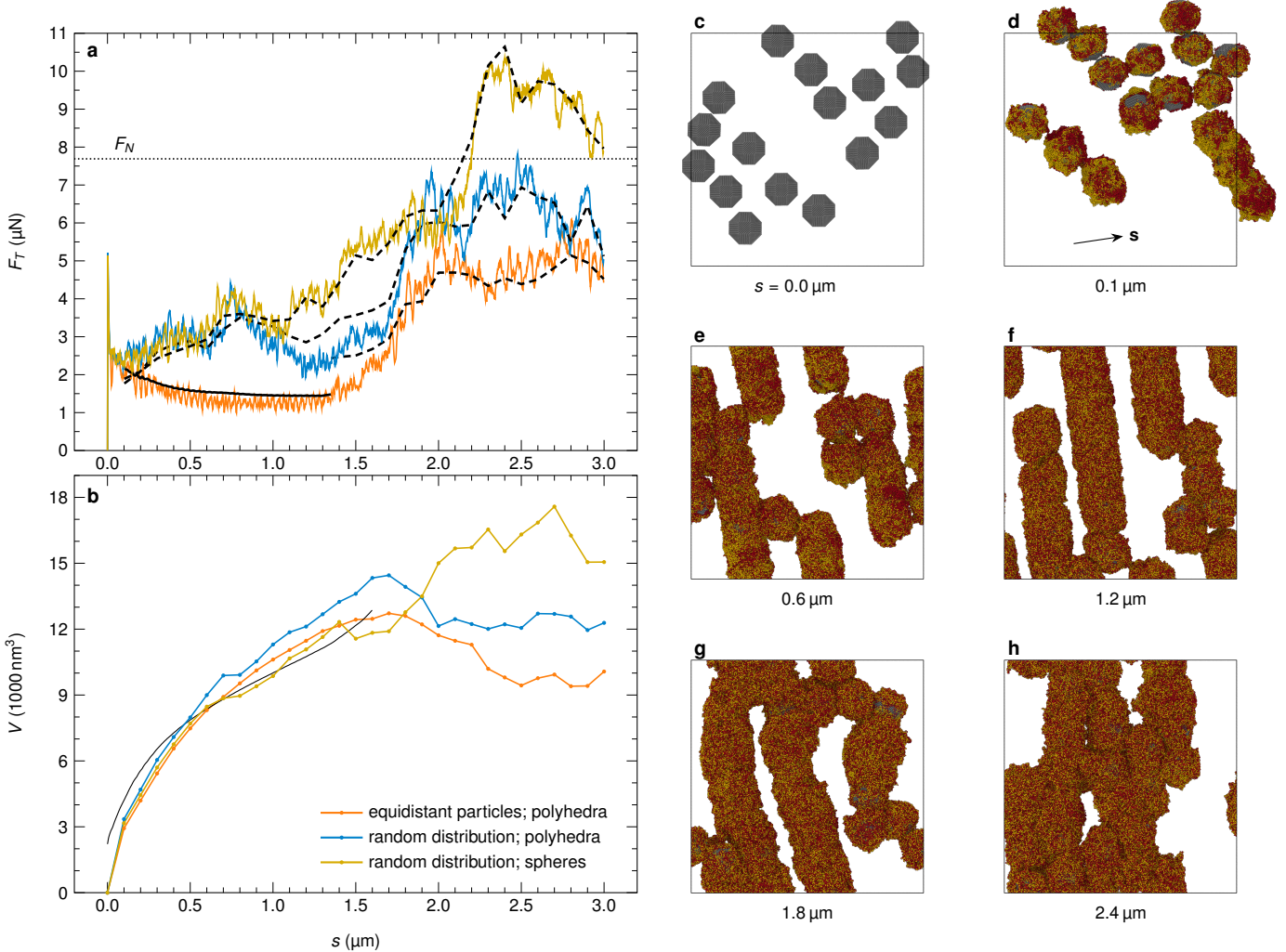
Figure S2: Influence of the initial particle placement. **a**, Compared to the regular arrangement with equidistant particles used for the main results (orange), random initial particle placement leads to an immediate transition to a high-friction regime. Solid black lines correspond to Eq. 1 in the main text, dashed black lines to Eq. 3. **b**, The wear rate does not immediately stagnate, though, as might be expected for the shear-band-like regime. A look at the morphology of the third body (panels **c–h**) can explain this: Parts of the system still clearly consist of rolling cylinders that continue to grow and pick up material. The wear rate only stagnates when all cylindrical particles strongly interact and/or merge (panels **g** and **h**). The solid black line in panel **b** corresponds to Eq. 6 in the main text, computed for the equidistant particles in the rolling regime.
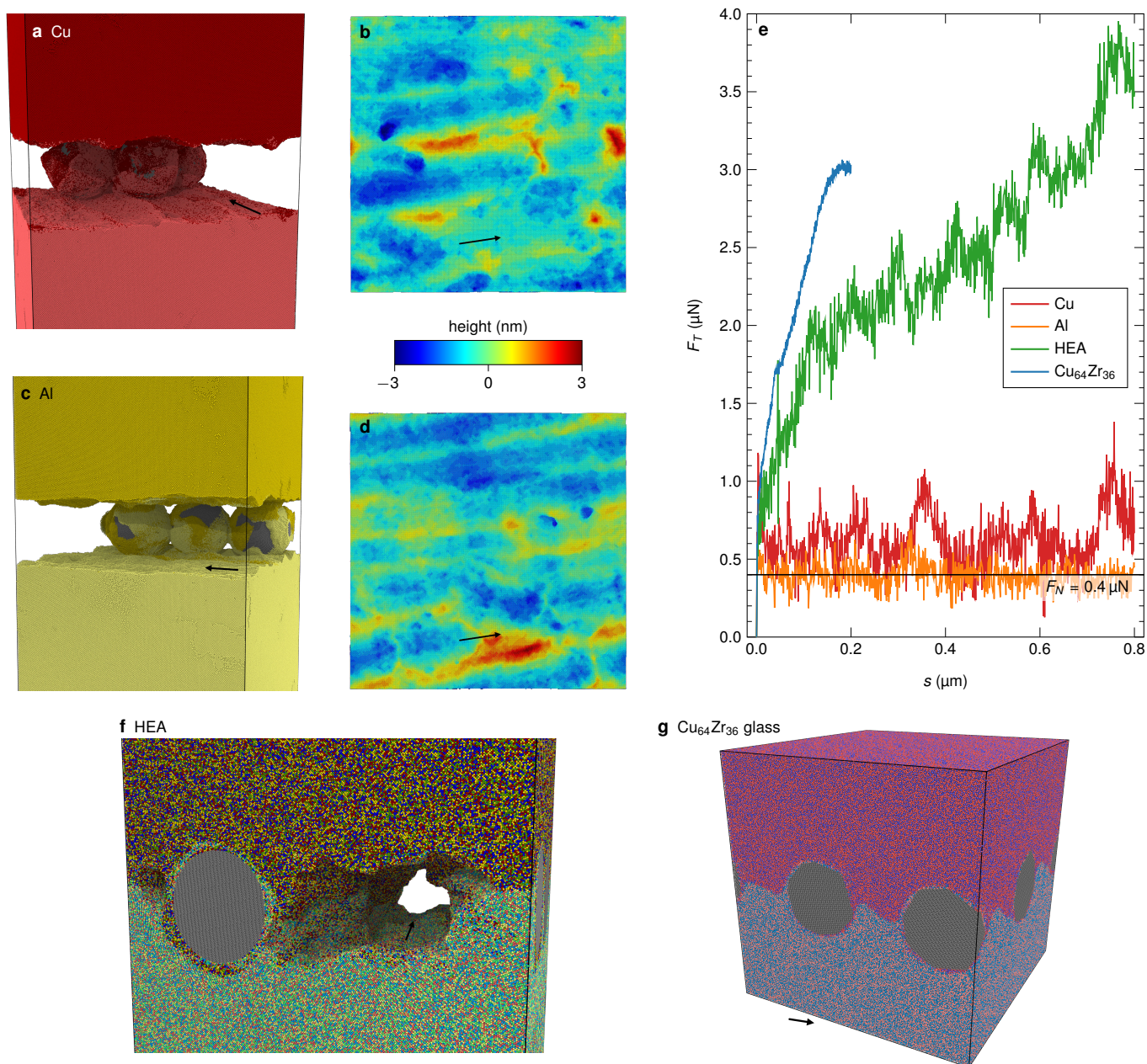
Figure S3: Sliding simulations on different metals. Copper (panels **a** and **b**) and aluminum (panels **c** and **d**) do not exhibit sustained rolling of the wear particles, but the particles stick together almost immediately, leading to scratching (see height maps in panels **b** and **d**) and friction coefficients of one or more (panel **e**). **f**, The high-entropy alloy shows more adhesion and plastic flow than the elemental metals, leading to large pickup of material and very quick welding. **g**, The metallic glass welds instantly due to strong softening of the surface.
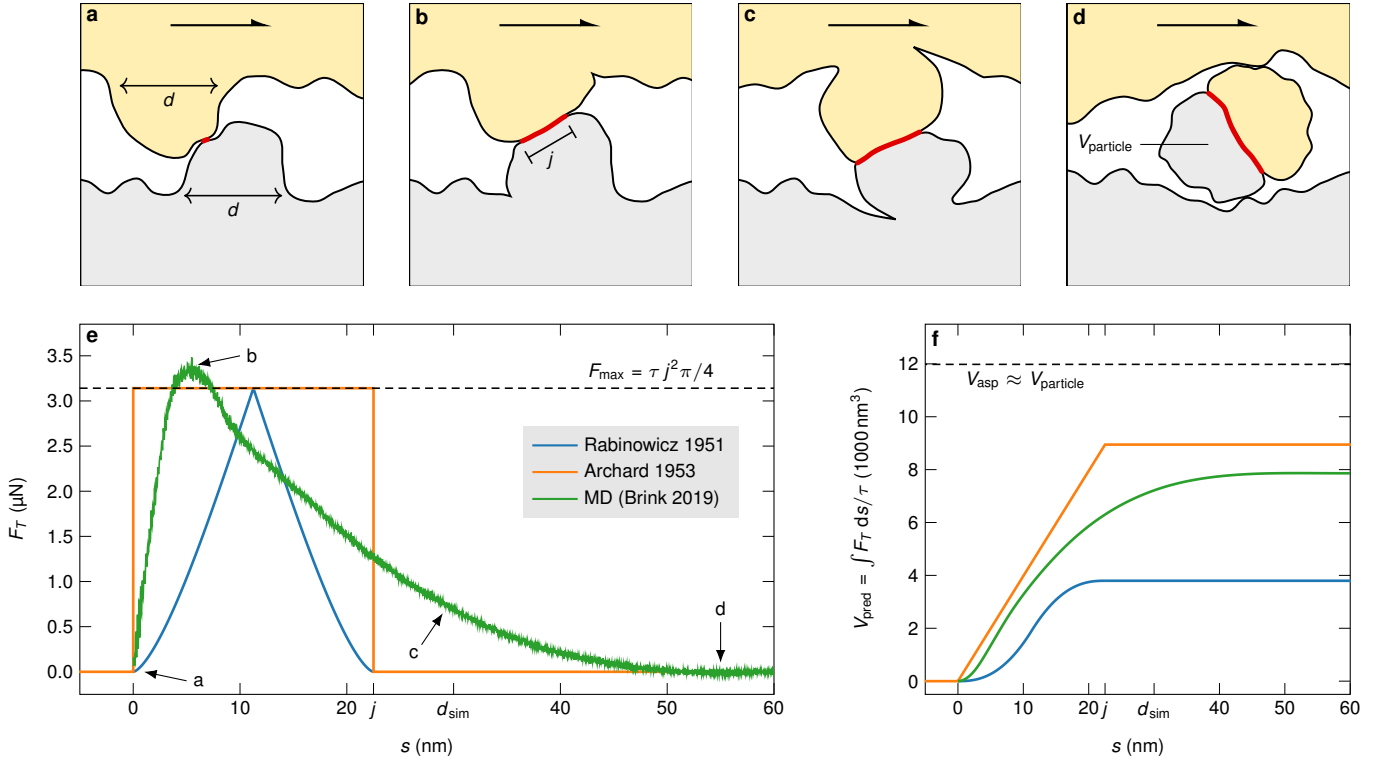
Figure S4: A single-asperity wear law. In the case of wear particle formation with significant plastic activity, it has been found that the wear volume in the single-asperity case is related to the tangential work by [1] $V = \int_0^s F_T \mathrm{d}s / \omega\tau \approx F_T s / \omega\tau$ (Eq. 5 in the main text), with ω being a shape factor close to unity. This single-asperity wear law can be derived by assuming that the asperity is loaded to its shear limit τ upon contact (panel **a**). During sliding, the particle starts to detach (panel **b** and **c**) and the full detachment (panel **d**) will take place at a sliding distance of $s = d$, where d is the asperity diameter, at which point F_T becomes negligible, allowing the approximation of a constant tangential force. The shear limit can be converted to the tangential force via $F_T = \omega\tau d^2$, assuming that the contact area is given by the asperity diameter ($j \approx d$). Measuring only the work $W = \int_0^s F_T \mathrm{d}s \approx F_T s$, one can estimate the asperity volume (and therefore the wear particle volume) via $s = d$ and $W/\tau = F_T d / (F_T / \omega d^2) = \omega d^3$. In this simple picture, all dissipation goes into forming a wear particle. In multi-asperity systems, additional frictional dissipation mechanisms occur, wherefore a wear coefficient k is introduced that takes into account that not all the tangential force is used for wear. **e,** Taking data from an earlier simulation study [2], we can compare the simple models of the tangential force profile by Rabinowicz [3] and Archard [4] with a particle-detachment simulation of a brittle material. As already indicated in panel **b**, the contact area is given by a contact diameter $j < d$, which we use here instead of d. **f,** We can also see that the measured wear volume (dashed line) exceeds the predictions, meaning that the wear process is more efficient. The reason is that a brittle asperity is not loaded to its shear limit in all of its volume, since brittle fracture can obviously occur before reaching the elastic limit. Nevertheless, the approximation reproduces the correct order of magnitude [1], as found before.
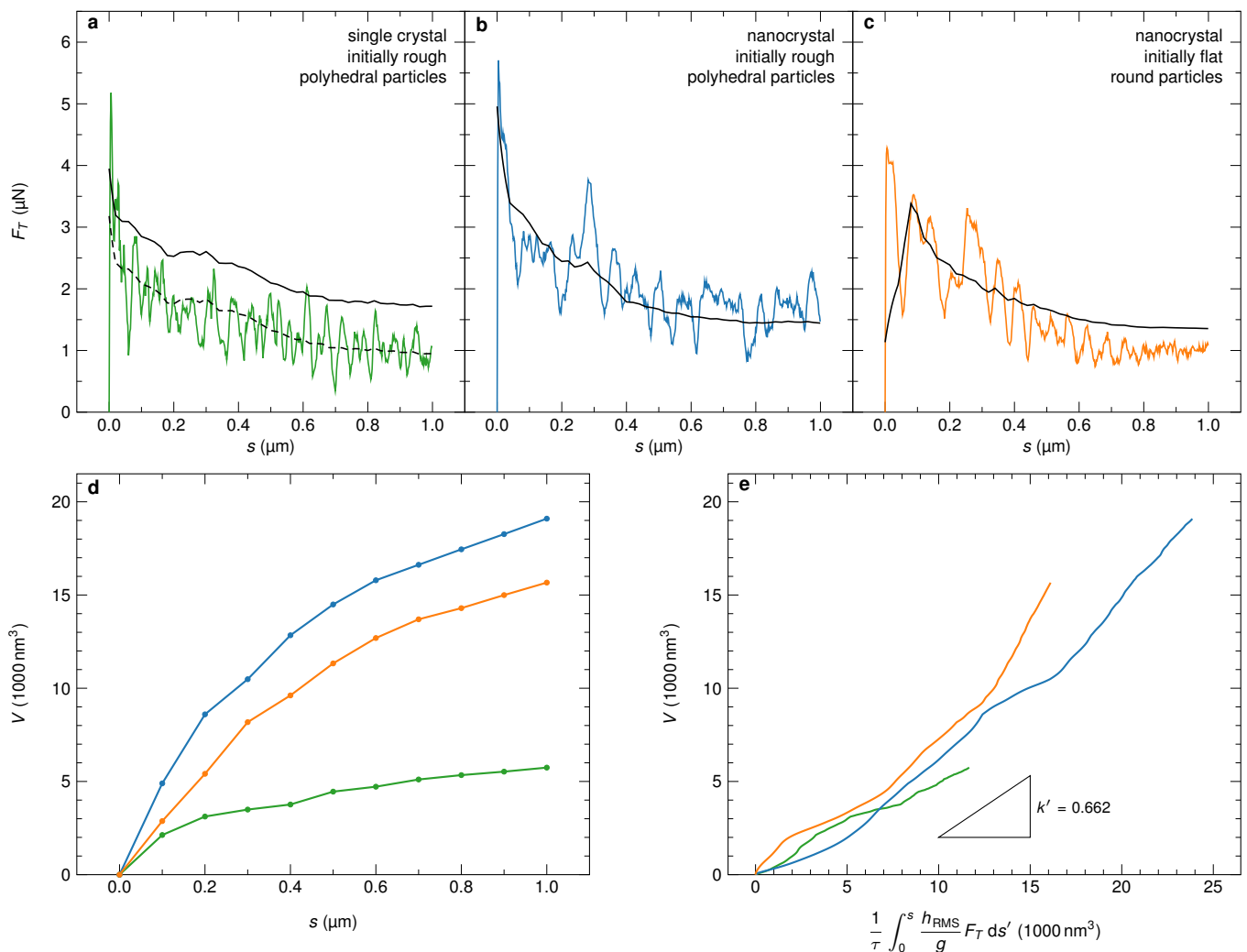
Figure S5: Friction and wear data of the same material used in the main text with four, large initial wear particles. The normal force was $F_N = 7.69\,\mu\mathrm{N}$. **a**, For the single-crystalline first bodies, the friction force (green line) is reduced compared to the prediction from the model in Eq. 1 in the main text (solid, black line). A fit (dashed, black line) can be achieved by reducing μ_0^r to 0.03. This indicates that the non-roughness contribution to the friction is lower, possibly due to a reduction of the contact area of the rollers (higher hardness of the single crystal) or due to a reduced effective shear strength (cf. Eq. 2 in the main text). The nanocrystalline first bodies starting from initially rough (panel **b**) and initially flat (panel **c**) surfaces follow the prediction using Eq. 1 in the main text (solid, black lines). **d**, In terms of wear volume, the single-crystalline system wears more slowly and the wear rates of both nanocrystalline systems are similar at the end. As expected, the initial wear rate for the rough surface is higher than for the flat surface. **e**, When plotting the wear volume over the wear prediction from Eq. 6 in the main text (cf. Fig. 4d in the main text), the curves collapse and we obtain approximately the same wear coefficient k' as before.
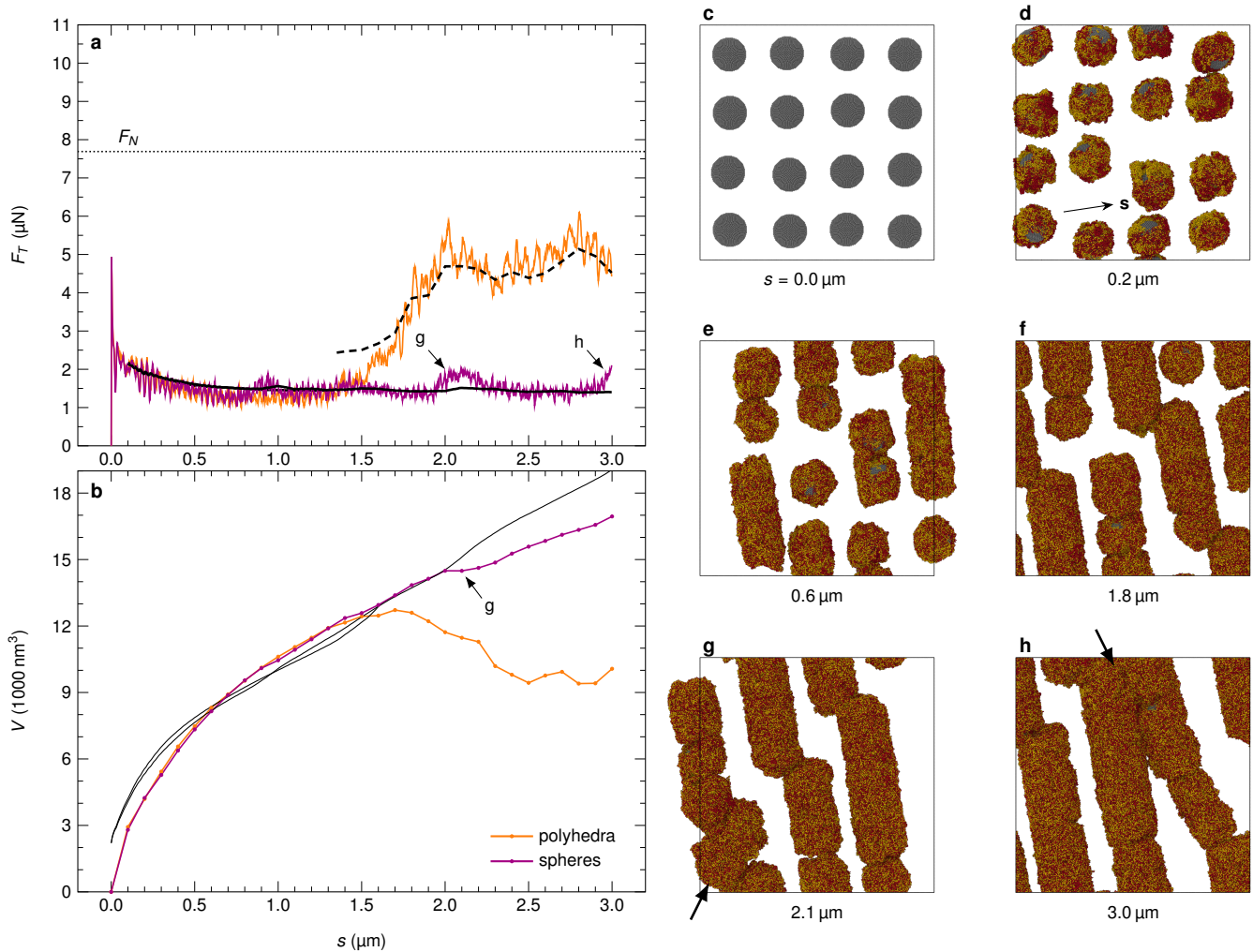
Figure S6: Influence of initial wear particle shape. We tested both polyhedral and round particles, but found that this does not significantly change either the friction (panel **a**) or the wear rate (panel **b**). This is because the particles are quickly coated by material picked up from the first bodies, resulting in the same shape after a short time in both cases. Solid black lines in panel **a** correspond to Eq. 1 in the main text, dashed lines to Eq. 3, and solid black lines in panel **b** correspond to Eq. 6. The only difference between the simulations is when the transition to the shear-band-like regime with high friction and low wear rate occurs. This transition is a stochastic process, though, and thus not a result of the initial particle shape. Panels **c–h** show the evolution of the third body starting from round particles. The rolling regime is retained throughout the simulation. Spikes in the friction can be connected directly to events where the rolling cylinders interact (panels **g** and **h**). Indeed, the transition to the shear-band-like regime seems to initiate already partially at around $s = 2\,\mu$m, where the wear rate becomes lower than the prediction for the rolling regime (panel **b**) and the particles start sticking together (panels **g** and **h**).
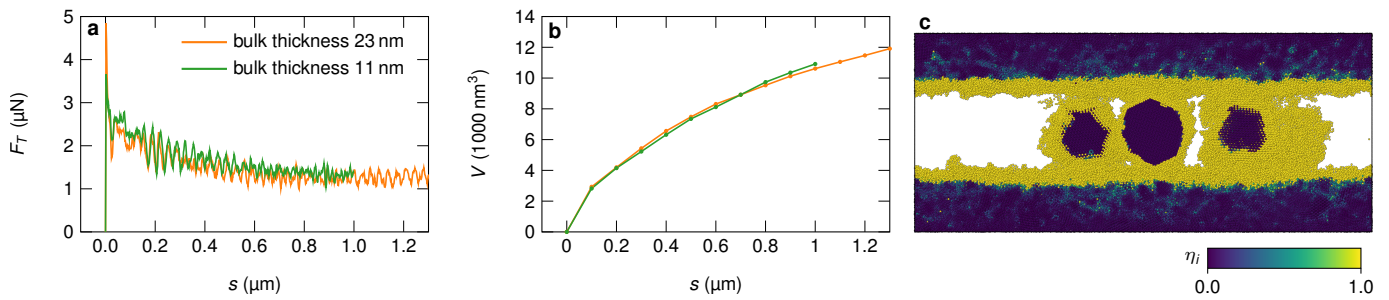
Figure S7: Verification that reducing the initial bulk height does not influence friction or wear within the simulated timescale. Since the system sizes in MD simulations are constrained due to the high computational demands of the method, finite size effects must be excluded. Here, we show that the friction (panel **a**) and wear (panel **b**) response of a system that is much smaller than those in the main results is the same. **c**, This can be explained by the fact that the plasticity, here visualized as the von Mises invariant η_i of the total atomic shear strain [5] at $s = 3\,\mu m$ for the sample with bigger initial bulk thickness, is quite localized at the surface.
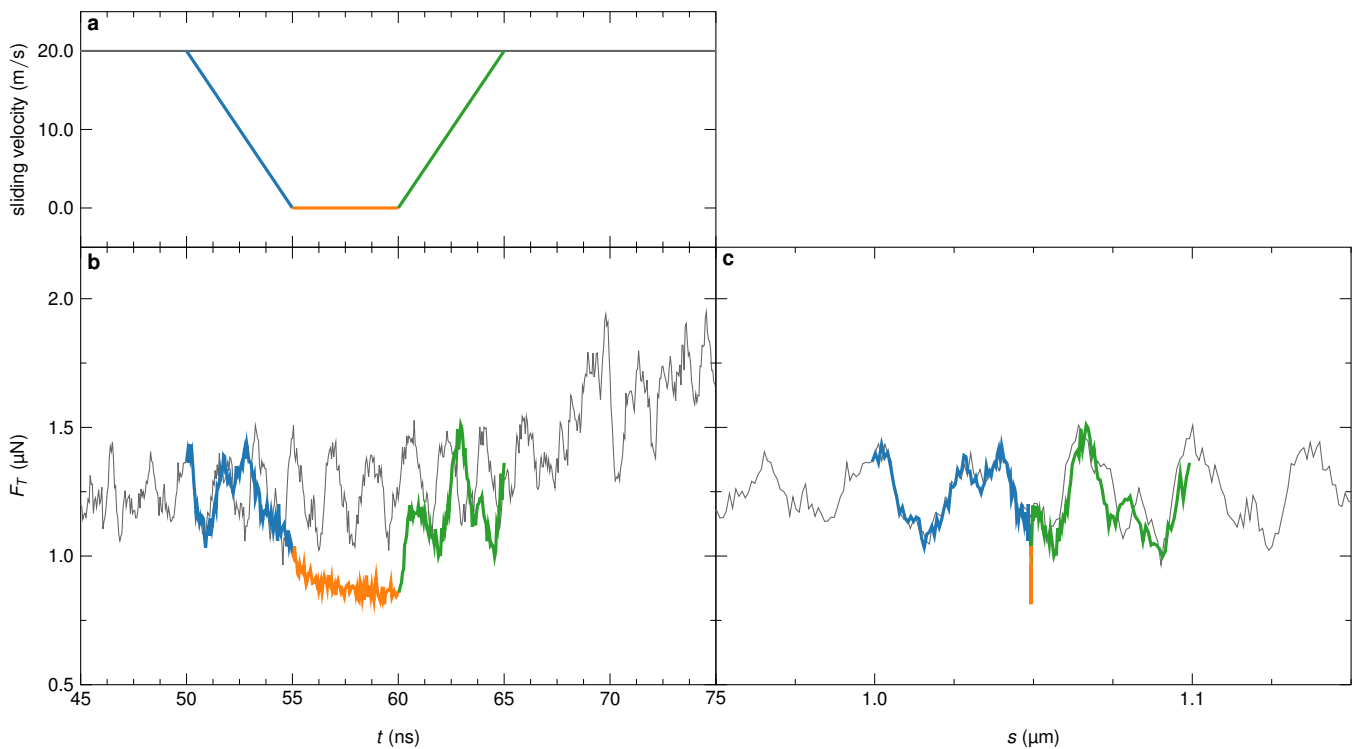
Figure S8: Change of the sliding velocity. **a**, We investigated the influence of the sliding velocity by restarting the sliding simulation with $F_N = 7.69\,\mu N$ at $s = 1\,\mu m$ but then slowly ramping down the velocity from 20 m/s to 0 m/s (blue), holding for 5 ns (orange), and ramping up the velocity again afterwards (green). Grey curves indicate the original, constant velocity simulation. **b**, The friction force relaxes during the holding period, but picks up again quickly afterwards. **c**, When plotting the same data over the sliding distance, it becomes clear that the friction response is not sensitive to the sliding velocity, but to the surface morphology.
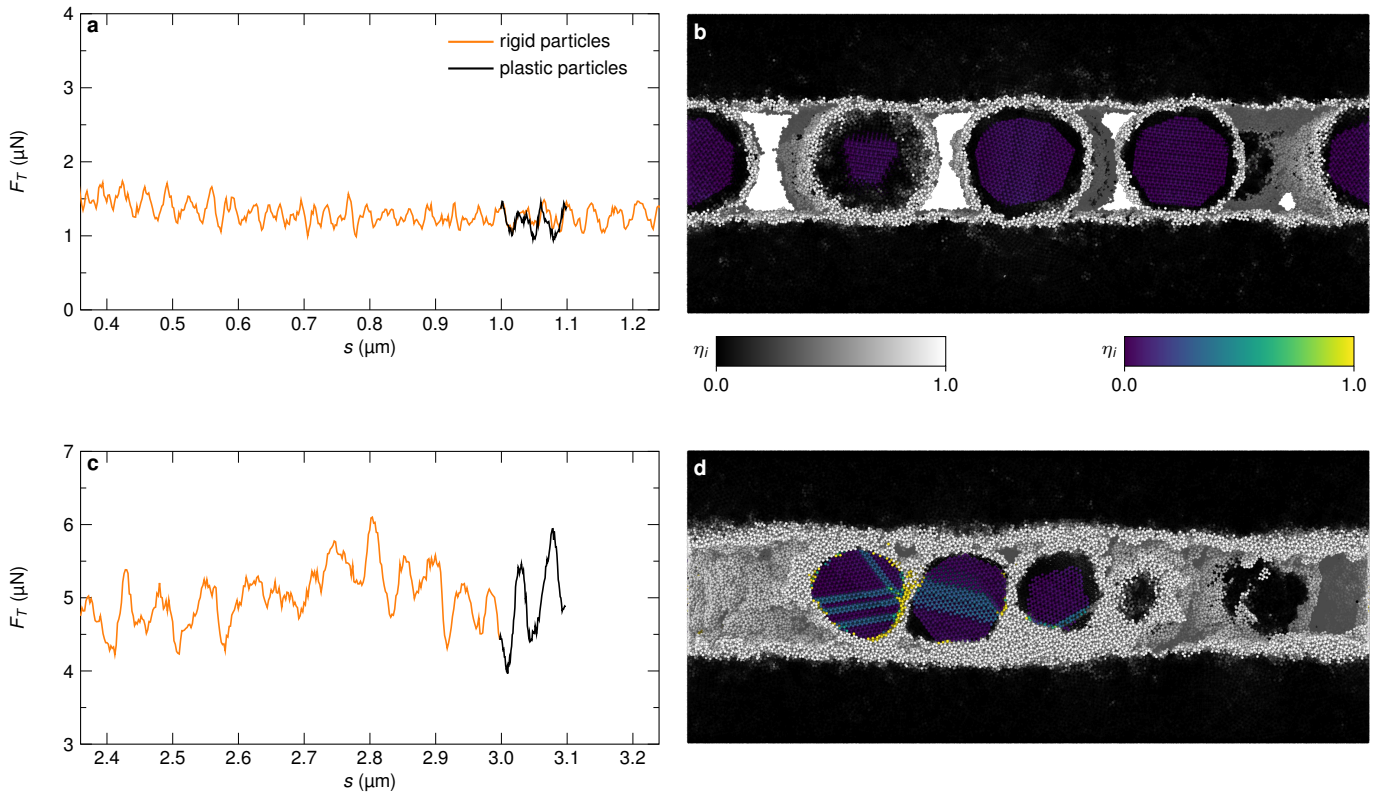
Figure S9: Making the abrasive particles non-rigid. **a**, Restarting the simulation with $F_N = 7.69\,\mu\text{N}$ at $s = 1\,\mu\text{m}$ in the rolling regime with non-rigid particles does not lead to any change in the friction force response. **b**, The atomic shear strain [5] (blue to yellow: originally rigid particles, black to white: rest of the system) shows no plasticity in the core of the wear particles. **c**, When continuing the simulation at $s = 3\,\mu\text{m}$, the friction force is also not affected by the rigidness of the particles. **d**, Nevertheless, plasticity can be observed inside the particles in accordance with the fact that the tribolayer is in a shear-band-like state. Here, shear forces get transmitted through the whole third body.

Supplemental references

[1] R. Aghababaei, D. H. Warner, and J.-F. Molinari, *On the debris-level origins of adhesive wear*, Proc. Natl. Acad. Sci. U.S.A. **114**, 7935–7940 (2017).

[2] T. Brink and J.-F. Molinari, *Adhesive wear mechanisms in the presence of weak interfaces: Insights from an amorphous model system*, Phys. Rev. Mater. **3**, 053604 (2019).

[3] E. Rabinowicz, *The nature of the static and kinetic coefficients of friction*, J. Appl. Phys. **22**, 1373–1379 (1951).

[4] J. F. Archard, *Contact and rubbing of flat surfaces*, J. Appl. Phys. **24**, 981–988 (1953).

[5] F. Shimizu, S. Ogata, and J. Li, *Theory of shear banding in metallic glasses and molecular dynamics calculations*, Mater. Trans. **48**, 2923–2927 (2007).